

Strong lensing of submillimetre galaxies: A tracer of foreground structure?

Gregory Paciga, Douglas Scott and Edward L. Chapin

Department of Physics & Astronomy, University of British Columbia, 6224 Agricultural Road, Vancouver, B.C., V6T 1Z1, Canada

9 February 2022

ABSTRACT

The steep source counts and negative K -corrections of bright submillimetre galaxies (SMGs) suggest that a significant fraction of those observed at high flux densities may be gravitationally lensed, and that the lensing objects may often lie at redshifts above 1, where clusters of galaxies are difficult to detect through other means. In this case follow-up of bright SMGs may be used to identify dense structures along the line of sight. Here we investigate the probability for SMGs to experience strong lensing, using the latest N -body simulations and observed source flux and redshift distributions. We find that almost all high redshift sources with a flux density above 100 mJy will be lensed, if they are not relatively local galaxies. We also give estimates of the fraction of sources experiencing strong lensing as a function of observed flux density. This has implications for planning follow-up observations for bright SMGs discovered in future surveys with SCUBA-2 and other instruments. The largest uncertainty in these calculations is the maximum allowed lensing amplification, which is dominated by the presently unknown spatial extent of SMGs.

Key words: submillimetre – gravitational lensing – galaxies: statistics – galaxies: high-redshift – cosmology: observations.

1 INTRODUCTION

Sources that are picked up in deep extragalactic millimetre (mm) and submillimetre (submm) wavelength surveys are far from being ordinary galaxies. Due to strong evolution, and also driven by the typically coarse angular resolution of current surveys at these wavelengths, mm/submm sources are rare and luminous compared with well-studied populations of optical galaxies. Submm galaxies (SMGs) are usually interpreted as an early rapidly star-forming phase, perhaps driven by a major merger, in the sequence that will ultimately become a massive elliptical galaxy (e.g., Blain et al. 2002, and references therein).

However, gravitational lensing can also play a role, such that some fraction of SMGs may be more typical, lower-luminosity galaxies at high redshift ($z > 1$) that are strongly amplified by lensing. This is already a well known effect for quasars, where the steepening source counts make lensing of increasing importance for the brightest objects (e.g., Kochanek 2006). In addition, the prevalence of giant optical arcs is partly explained by the high redshifts of the sources (Wu & Chiueh 2006). There are many anecdotal examples of SMGs that are either known or strongly suspected to be lensed. Examples include sources seen through targeted rich galaxy clusters, most spectacularly in Abell 2218 (Kneib et al. 1996; Swinbank et al. 2003), and MS0451-03 (Borys

et al. 2004), as well as the brightest source in the central Hubble Deep Field North, usually called HDF850.1 (Dunlop et al. 2004), the brightest source in the entire GOODS-North field, referred to as GN20 (Pope et al., submitted), and other bright well-studied sources, such as SMM J14011+0252 (Ivison et al. 2001; Smail et al. 2005), MIPS J142824.0+352619 (Borys et al. 2006), and SMM J02399-0136 (Ivison et al. 1998). It has long been recognized (e.g., Blain & Longair 1993) that the steep source counts and high redshifts of SMGs make the brightest ones prime lensed candidates.

Despite some efforts to model the lensing contribution to the source counts (e.g., Perrotta et al. 2002, 2003; Negrello et al. 2007) the predictions for SMG lensing are still very uncertain. The purpose of the present paper is to improve this situation, using the latest numerical models, and to try to quantify the uncertainties. In the process of this investigation we will also be able to address a related question – namely whether bright SMGs could be used as tracers of galaxy clusters at redshifts that are high enough to be challenging for other techniques.

In order to carry out this study we will need several ingredients, including the unlensed submm source counts and the redshift distribution. However, we start in section 2 by considering the probability distribution for lensing amplification along random lines of sight. We then look at the observed and modelled source counts for SMGs in section 3

and use these to calculate the source counts after lensing in section 4, also exploring the dependence on the redshift distribution of sources. A major simplification of our approach is to assume that the *shape* of the source counts is independent of redshift; in order to test this we calculate in section 6 lensing expectations from a specific evolutionary model that is consistent with a range of current IR and sub-mm data. Finally, we consider the uncertainties in the various components of our analysis in section 5 and interpret our results in the context of upcoming submm surveys in section 7.

2 PROBABILITY DENSITY FUNCTION

2.1 Millennium Simulation

The first ingredient we will need for our study is the statistical distribution of lensing amplifications. Wang et al. (2002) presented a ‘universal probability distribution function’ valid for all cosmologies and redshifts. However, it is only applicable to weak lensing, with a maximum magnification much less than 10. As we are interested in strong lensing effects leading to the very brightest sources, where we will find a mean magnification far beyond the weak lensing regime, this is unsuitable for our purposes. Other relevant studies (Perrotta et al. 2002; Negrello et al. 2007) have used largely analytic approximations, have also focused on weak lensing (Jain et al. 2000; Keeton et al. 2005), or have relied on N -body simulations (Bartelmann & Weiss 1994; Wambsganss 1992) which have since been dwarfed in size by the Millennium Simulation (Springel et al. 2005), a computational run containing approximately 10^{10} particles of mass $8.6 \times 10^8 M_\odot/h$ in a cube of side 500 Mpc/ h .

Hilbert et al. (2007) studied lensing amplification probability distributions using a ray tracing approach with the Millennium Simulation, and a Λ CDM cosmology with parameters $\Omega_M = 0.25$, $\Omega_\Lambda = 0.75$, $h = 0.73$, $n = 1$, and $\sigma_8 = 0.9$. They calculate optical depths τ_μ^I and τ_μ^S for an image having been magnified by a factor μ . The former gives the optical depth assuming a uniform distribution of images, whereas the latter assumes a uniform distribution of sources. Since we are lensing an approximately random background of submm galaxies, henceforth we will use only τ_μ^S and its related probability density function (PDF) $p^S(\mu)$, omitting the superscript ‘S’ from now on.

Notice that this is not strictly the probability for a source undergoing a total magnification μ , but only for one image of a source. There is some ambiguity here over whether we should be considering the total amplification for all images – this will depend on how SMGs are detected, the resolution of the imaging and on details of individual lensing models. Having pointed out this ambiguity, we will simply ignore it for the rest of the paper.

Given $p(\mu)$, the probability that a source has been amplified by a factor μ in the range $(\mu, \mu + d\mu)$ is then $p(\mu)d\mu$. Though the scalar magnification μ has a sign associated with it, where negative values indicate a change in image polarity (for a review see, e.g., Schneider et al. 1992; Courbin et al. 2002), the behaviour of the PDF at $\mu < 1$ will allow us to take $\mu > 0$. We will require that the PDF be normalised:

$$\int_0^\infty p(\mu)d\mu = 1. \quad (1)$$

Since flux of a source must be conserved, sources amplified in some directions must be deamplified in others. This flux conservation constraint takes the form (Hilbert et al. 2007)

$$\int_0^\infty |\mu|p(\mu)d\mu = 1. \quad (2)$$

The ray tracing techniques used essentially assume point sources, which allows for arbitrarily high magnifications. The consideration of extended objects imposes a maximum magnification limit, estimated by Perrotta et al. (2002) to be in the range 10–30 for 1–10 kpc sources at redshifts 1–4. The applicability of this estimate to SMGs, however, is uncertain, since the characteristic size of emission is unknown. SMGs appear to be extended objects of a few kpc, but may well be clumpy (Pope et al. 2005; Chapman et al. 2003), so small knots of bright star-formation would have a higher potential for amplification by lensing than the galaxy considered as a whole. Perhaps the best empirical constraint comes from Younger et al. (2007), who recently constrained the sizes of the submm emitting regions to $\lesssim 10$ kpc using interferometry. Until we have much more concrete information about the size distribution of SMGs there is little we can do about the effects of finite source size. For now we continue without a maximum magnification limit, but will consider in section 5.1 how imposing such a constraint would affect our results.

2.2 Transform to other redshifts

Hilbert et al. (2007) give numerical data for a source plane at $z = 2.1$, as well as the peak position $\mu_p(z)$ and full width at half maximum FWHM(z) of the distributions for other redshifts. We found that we could transform the $z = 2.1$ PDF to other redshifts using a transformation of the form

$$\mu \longrightarrow \mu' = \left(\frac{e^{b/\mu_p} - 1}{e^{b/\mu} - 1} \right) \mu_p + \delta\mu_p, \quad (3)$$

$$p(\mu) \longrightarrow p'(\mu) = Ap(\mu), \quad (4)$$

where μ_p is the peak amplification at the reference z , $\delta\mu_p$ is the shift in the peak between redshifts, b is determined by requiring that we obtain the correct FWHM, and the normalisation constant A is determined by requiring that we satisfy equation (1). The peak shifts to lower μ as z increases, to balance the high μ tail, allowing the PDF to satisfy equation (2).

This transformation preserves the asymptotic behaviour of the PDF, as discussed in section 2.3, which is most crucial to our analysis. We plot the resulting family of curves in Fig. 1. For reference the values of the coefficients are $(A, b) = (0.473, -1.504)$, $(0.968, -0.051)$, $(1.383, 0.655)$, $(1.681, 1.077)$ and $(1.889, 1.346)$ for $z = 1, 2, 3, 4$ and 5 , respectively.

2.3 Limiting behaviour

The PDF for $z = 2.1$ is seen to have a μ^{-3} tail, as predicted by theory (Schneider et al. 1992) above an amplification of about $\mu_{\text{high}} \simeq 20$. Thus, the data are fit to

$$p(\mu) = A_{\text{high}}\mu^{-3} \quad \text{for } \mu > \mu_{\text{high}}, \quad (5)$$

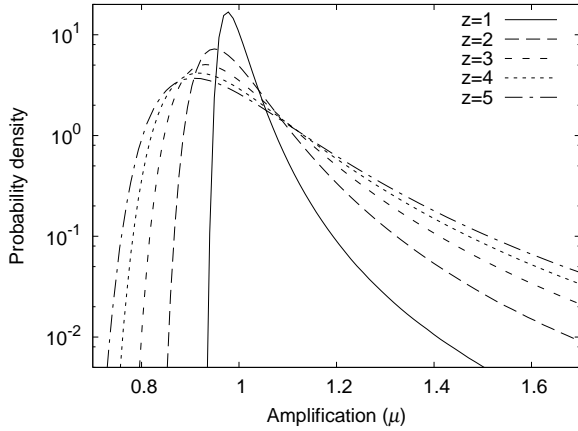


Figure 1. Family of lensing amplification PDF curves at different source redshifts, derived from Hilbert et al. (2007).

where A_{high} is an adjustable parameter, and this functional form can be used to extend the PDF to arbitrarily high amplifications. The μ_{high} limit is adjusted for all other redshifts according to the transformation described above. Inaccuracy in the μ^{-3} behaviour above this limit may cause a small kink in the function at the transition between the data and the extrapolation, but we find this to be quite small.

In the Hilbert et al. (2007) data for $z = 2.1$ there is a cut-off at about $\mu = 0.8$, where the PDF stops decreasing and reaches a near constant plateau. In this paper we are not interested in the deamplification effects from the $\mu < 1$ regime, so at most this low- μ behaviour is important only for the normalisation of the PDF. We find that by instead allowing the PDF to drop off like a Gaussian the normalisation of the PDF is changed by about 10^{-6} , and so is negligible for our purposes. We therefore assume that the PDF goes to zero like a Gaussian for small μ , i.e.,

$$p(\mu) = A_{\text{low}} \exp\left(-\frac{(\mu - \mu_0)^2}{2\sigma^2}\right) \quad \text{for } \mu < \mu_{\text{low}}, \quad (6)$$

where A_{low} , μ_0 , and σ are adjustable parameters, and here μ_{low} is chosen to make as smooth a transition from the data to the Gaussian as possible. The peak of the distribution itself remains defined by the data. For example, for $z = 2.1$, the peak of the distribution is at $\mu \simeq 0.95$, while the low Gaussian tail is not used until $\mu < \mu_{\text{low}} = 0.8$.

This approach is in contrast to Perrotta et al. (2003) who approximated the entire weak lensing regime below $\mu \simeq 1.5$ – 2.0 as a Gaussian and the entire strong lensing regime above the same limit by the μ^{-3} power-law. Our approach is to use numerical data for a broad intermediate range, giving a more accurate shape for the PDF, particularly for small and intermediate amplifications.

3 SOURCE COUNTS

3.1 Fits to observed counts

Functional fits to observed differential source counts of submillimetre galaxies are given in Coppin et al. (2006), derived from the SCUBA Half Degree Survey (SHADES) at $850 \mu\text{m}$. They use both a broken power-law of the form

$$\frac{dN}{dS} = \begin{cases} \frac{N'}{S'} \left(\frac{S}{S'}\right)^\alpha & \text{if } S < S', \\ \frac{N'}{S'} \left(\frac{S}{S'}\right)^\beta & \text{if } S > S', \end{cases} \quad (7)$$

and a Schechter functional form

$$\frac{dN}{dS} = \frac{N'}{S'} \left(\frac{S}{S'}\right)^{\alpha+1} e^{-S/S'}. \quad (8)$$

with units of $\text{mJy}^{-1}\text{deg}^{-2}$. The differential counts dN/dS can be integrated from S to infinity to obtain the cumulative counts $N(>S)$ with units of deg^{-2} . Currently there are not enough high flux ($S > 20 \text{ mJy}$) sources to prefer one function over the other.

We have chosen to use the Schechter function as our primary estimate of the source counts. The power-law drops off much slower than the exponential part of the Schechter function, allowing for many more intrinsically bright objects. As such, the most gradual power-law consistent with the data can be used as an upper estimate to the counts, which results in a far more conservative estimate of the strong lensing probabilities. A lower limit to the source counts is less helpful, as the corresponding uncertainty in the upper limit of lensing probabilities is unknown.

The Schechter function parameters that we adopt are, in parallel with Coppin et al. (2006), $N' = 1600$, $S' = 3.3$, and $\alpha = -2$. For the maximal broken power-law we use $N' = 58$, $S' = 9$, $\alpha = -2.2$, and $\beta = -4.2$. The contribution to the overall background (i.e. $\int S(dN/dS)dS$) from a power-law number counts distribution diverges at the faint end if the slope $\alpha \leq -2$ (in equation (7)). To prevent overproducing the submm background, we therefore set a limit on the broken power-law of $S \geq 0.2 \text{ mJy}$.

3.2 Phenomenological models

Lagache et al. (2003) used a phenomenological approach to model galaxy evolution and predict number counts at a variety of wavelengths, including $850 \mu\text{m}$, and corrected this to include constraints from *Spitzer* data in 2004. Their standard model is roughly consistent with Coppin et al. (2006) in the range where data from SHADES exist, but decreases much more slowly above about 50 mJy . This is due entirely to local bright Euclidean counts, for which $dN/dS \propto S^{-5/2}$. Chary & Elbaz (2001) similarly have a model for the source counts that has been adjusted to include the *Spitzer* data. The results of their model at $850 \mu\text{m}$ is very similar to Lagache et al. (2004), including the bright Euclidean part as well.

Normalising a Euclidean source count estimate to the SCUBA Local Universe Galaxy Survey (SLUGS; Dunne et al. 2000), we find agreement with the high flux behaviour in both the Lagache et al. (2004) and Chary & Elbaz (2001) models. Since the Euclidean part of the source counts comes from low redshift sources, we do not expect there to be any significant lensing here. Subtracting the $S^{-5/2}$ part from either of these models to estimate the high redshift population, we find that the high flux fall-off is very similar to a Schechter function. This is only a first-order approximation, as in principle the source counts change for each redshift slice. We will investigate redshift dependence in section 4.2 and the change in the shape of the counts with redshift in 5.2. We will also compare with the results from an evolu-

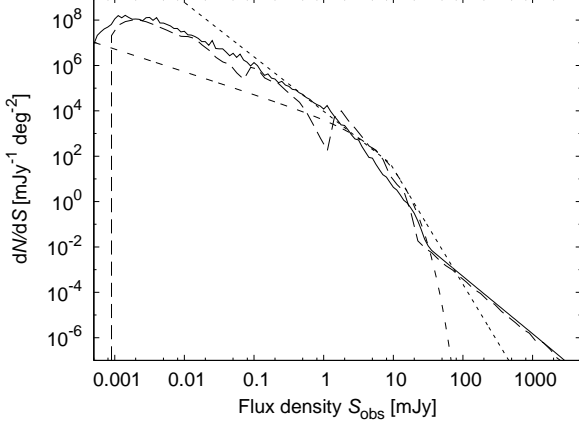


Figure 2. Differential number counts prior to applying lensing. Solid and long-dashed lines are the models of Lagache et al. (2004) and Chary & Elbaz (2001), respectively. Short-dashed and dotted lines are the Schechter functional form and broken power-laws from Coppin et al. (2006).

tionary model in section 6. But for now we will assume a single screen of sources with counts independent of redshift.

Between the low flux limit of the models at about $1 \mu\text{Jy}$ and the knee at several mJy, both models predict intermediate counts between the Schechter and broken power-law fits. Fig. 2 compares these functional fits to the models of Lagache et al. (2004) and Chary & Elbaz (2001). This justifies our use of the Schechter and power-law functional forms as our ‘best’ and ‘maximal’ estimates, respectively. The lensed source count estimates in this paper at high flux densities should be considered to be *in excess of* known local (e.g., *IRAS*) galaxies, unless otherwise stated. We will see that, as expected, highly amplified sources make an increasing contribution at brighter fluxes.

4 CALCULATING LENSING EFFECTS

4.1 Observed source counts

If an object with flux density S is amplified through lensing by a factor μ , the object is observed with flux density $S_{\text{obs}} = \mu S$ (Schneider et al. 1992). For a given observed flux S_{obs} , we run through a range of magnifications, find the corresponding S , and assign $p(\mu)dN/dS$ to be the contribution to the lensed differential source counts from that μ . In this way we can express the differential source counts after lensing as

$$\frac{dN}{dS_{\text{obs}}}(S_{\text{obs}}) = \int_0^\infty \frac{dN}{dS} \left(\frac{S_{\text{obs}}}{\mu} \right) p(\mu) d\mu. \quad (9)$$

For different values of S_{obs} we plot the contribution to the above integral as a function of μ in Fig. 3. We do this specifically for sources at $z = 2$, as well as showing a separate panel with results normalised by the total contribution from all μ . In the normalised case, the line can be interpreted as a local $p(\mu)$ for that S_{obs} . Although we have only plotted results for $z = 2$, other redshift choices look qualitatively similar.

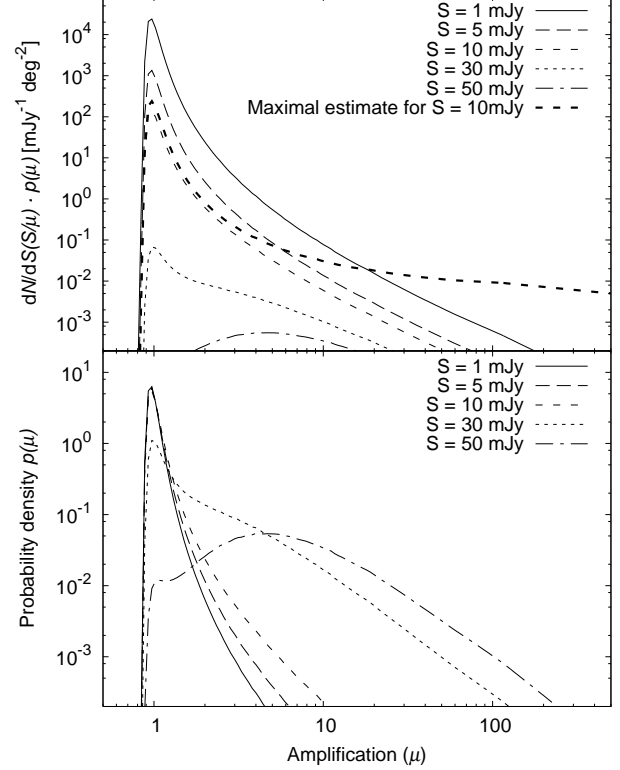


Figure 3. Magnification distributions. The contribution to dN/dS_{obs} made by each μ for various S_{obs} at $z = 2$ (top) and normalised by the total dN/dS_{obs} (bottom). The bottom panel shows how the high μ tail dominates over the $\mu \simeq 1$ peak for all $S \gtrsim 30 \text{ mJy}$. The additional thick line in the top panel is the ‘maximal’ estimate for $S_{\text{obs}} = 10 \text{ mJy}$ (the difference is typical for all S_{obs}).

We can also examine the contribution to the source counts coming from various magnifications by specifying a minimum μ that we might be interested in. The fractional contribution to dN/dS_{obs} from $\mu > \mu_{\text{min}}$ is found simply by changing the lower limit on the integral in equation 9 from 0 to μ_{min} , and normalising by the full dN/dS_{obs} . This is plotted in Fig. 4. It can be seen that at high flux densities a large portion of sources will have significant amplifications.

4.2 Comparing Redshifts

Lensing PDFs and a dN/dS function can be combined at arbitrary redshifts in the range $0.5 < z < 5.7$ (where Hilbert et al. (2007) quantify their lensing simulation). The differential source counts of the lensed populations are found via equation 9 and shown in Fig. 5 for a range of source redshifts. One can see that the lensing tail is relatively important above about 20 mJy and more so for higher redshift submm galaxies.

The cumulative source counts,

$$N(> S) = \int_S^\infty \frac{dN}{dS_{\text{obs}}} dS_{\text{obs}} \quad (10)$$

are used to determine the density of sources above a given flux on the sky. This is a useful quantity for making observational predictions for surveys.

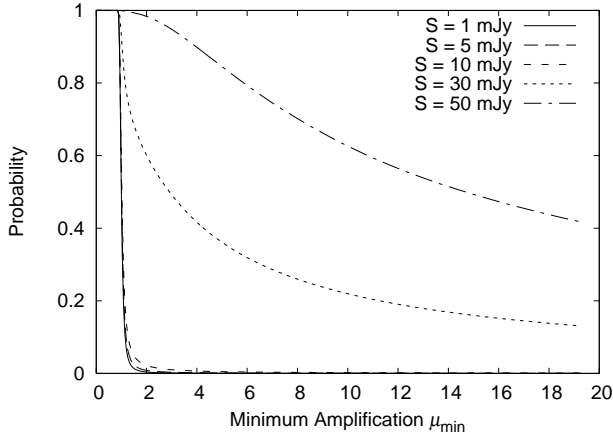


Figure 4. Combined contribution to dN/dS_{obs} from all magnifications above μ_{min} for sources at $z = 2$.

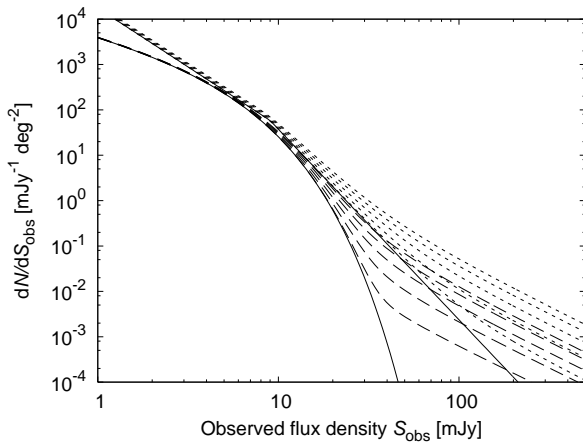


Figure 5. Lensed differential source counts found using equation 9. Dashed lines represent counts derived from the best Schechter function (lower solid line) and dotted lines those from the maximal power-law (upper solid line). Each set of curves is for sources placed at $z = 1, 2, 3, 4$, and 5 from bottom to top.

Examining the contribution to source counts as a function of μ_{min} , as described above, we set, somewhat arbitrarily (though consistent with Negrello et al. 2007 and Perrotta et al. 2002), a characteristic magnification for lensing events of $\mu_{\text{min}} = 2$. In Fig. 6 we plot the contribution as a function of S_{obs} for various redshifts, as well as the ‘best’ and ‘maximal’ estimates for the average over all redshifts. This quantifies the probability that an object observed at some S_{obs} has been lensed with a magnification greater than 2. One could easily obtain similar results for any other choice of minimal amplification.

There have been several attempts to characterise the redshift distribution of SMGs. Though phenomenological models do exist (e.g., Granato et al. 2001) we focus on estimates based purely on observational data. Chapman et al. (2005) obtained a large number of spectroscopic redshifts for radio selected galaxies, while Pope et al. (2006) obtained both spectroscopic and photometric redshifts in the GOODS-North survey, and Aretxaga et al. (2007) used radio/submm photometric redshifts in the SCUBA Half De-

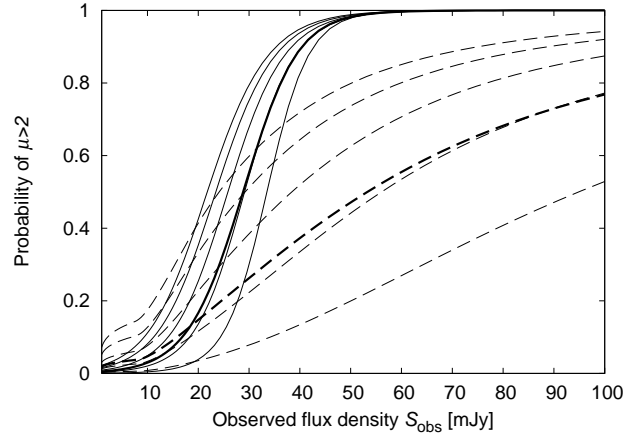


Figure 6. The fraction of dN/dS_{obs} due to magnifications greater than 2, which can be interpreted as the probability of a lensing event as a function of S_{obs} . The solid lines use the Schechter source counts and dashed lines use the maximal broken power-law, resulting in a minimal estimate of the lensing probability. We show (from bottom to top) $z = 1, 2, 3, 4$, and 5 as thin lines and the average over all redshifts as a thick line in each case.

gree Survey (SHADES). All three are consistent with a Gaussian distribution centred at $z = 2.2 \pm 0.1$ and with $\sigma = 0.8 \pm 0.1$. This is the distribution we use to obtain the average over redshift in Fig. 6. The results are nearly identical when varying the peak redshift by ± 0.1 . Fig. 6 shows that for sources with $S_{\text{obs}} \simeq 20$ mJy the probability of strong lensing is already 10–20 per cent for any reasonable redshift distribution. Empirical evidence suggests that this may be a conservative estimate, since at the moment all sources detected with $S_{\text{obs}} \gtrsim 20$ mJy at $850 \mu\text{m}$ have been claimed to be lensed.

We can also look at the average amplification as a function of observed flux density, given by

$$\langle \mu \rangle = \frac{\int_0^\infty \mu \frac{dN}{dS}(S_{\text{obs}}/\mu) p(\mu) d\mu}{\int_0^\infty \frac{dN}{dS}(S_{\text{obs}}/\mu) p(\mu) d\mu}. \quad (11)$$

This is shown in Fig. 7 across a range of redshifts. One can see a change in behaviour at higher and lower flux densities, depending on the source redshift. Below about 35 mJy the mean amplification increases with redshift, while above 35 mJy it decreases with redshift. This is due to the change in dominance between the $\mu \simeq 1$ peak and the high μ tail, an effect that can be seen in the bottom panel of Fig. 3.

5 UNCERTAINTIES

5.1 Lensing probabilities

Hilbert et al. (2007) discuss how they may have underestimated the lensing properties by about 15 per cent, based on replacing the principle lensing objects in their ray tracing by analytical haloes of the Navarro, Frenk & White (1997) form. This is surely a conservative estimate of the effects since baryons are neglected. Most large-scale simulations, like the Millennium Simulation, include only collisionless dark matter and not the much more complicated dissipative baryons. Clumping due to baryons is bound to increase

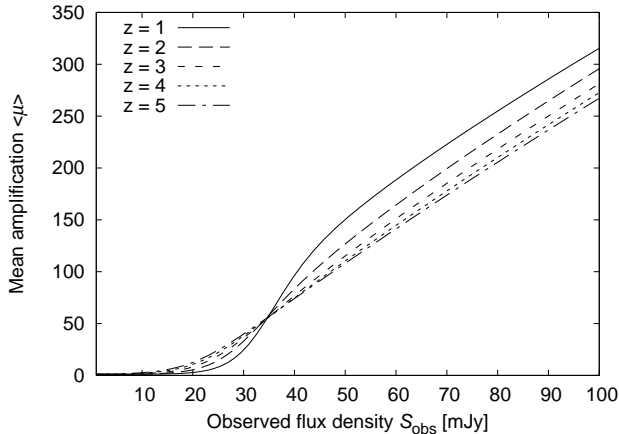


Figure 7. Mean magnification as a function of S_{obs} .

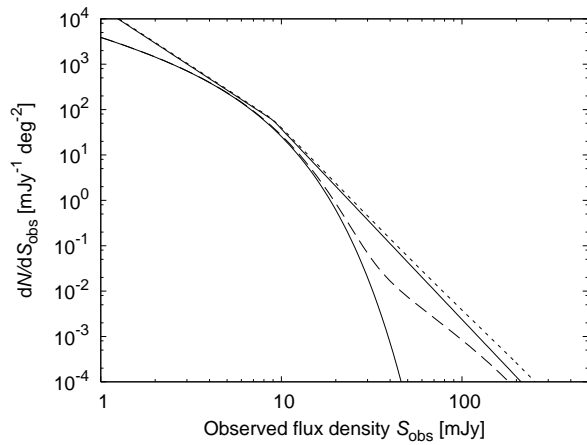


Figure 8. Differential source counts including the effects of lensing, *but* with a hard upper limit on the amplification of $\mu < 30$. Here we have plotted lensed counts for the Schechter (dashed) and power-law (dotted) models, for the average over all source redshifts. This should be compared with Fig. 5, making it clear how dramatic the effects are at the bright end.

strong lensing (e.g., Bartelmann et al. 1995) and so the normalisation of the high μ tails that we use should be considered as a lower limit. Recent studies (e.g., Wambsganss et al. 2008; Hilbert et al. 2008) suggest that structure due to baryon cooling and dissipation increase the incidence of strong lensing by at least 25 per cent.

However, the effect of finite source size goes in the opposite direction. For extended sources there is an upper limit on the magnification, as mentioned in section 2. The effect of this on the lensing probabilities can be significant, depending on the counts and on details of the size distribution. We can use Fig. 7 to gauge how important this might be. If we expect the limit to be ~ 30 , then the effect will be negligible for sources with $S_{\text{obs}} \lesssim 30$ mJy, but increasingly important for brighter sources.

We further show the importance of such a cut-off in Fig. 9, where we have calculated the differential source counts using the lensing PDF, but not allowing any events at $\mu > 30$. One can see significant changes for the brightest counts compared with Fig. 5. We also show the changes in

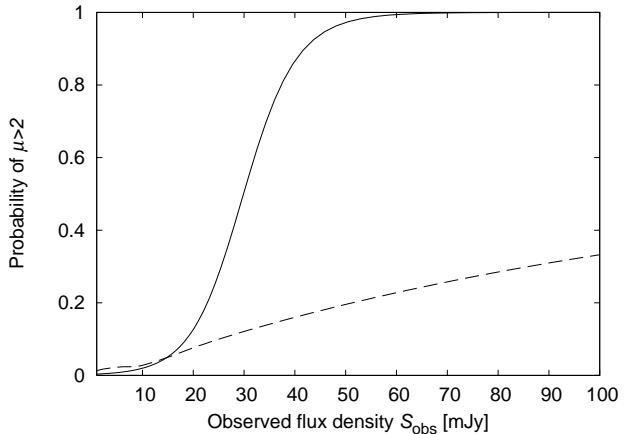


Figure 9. Fraction of the differential counts having amplification $\mu > 2$, but restricted to lensing distributions with maximum of $\mu = 30$. Here we plot the results for the Schechter (solid) and power-law (dashed) counts models for the average over all source redshifts. This plot should be compared with Fig. 6.

the probability of strong lensing as a function of observed flux density in Fig. 6, again using a maximal amplification of $\mu = 30$. One can see that the fraction of strongly lensed sources is significantly reduced, particular for the power-law counts model.

Is 30 a reasonable limit for lensing amplification? One indication that there is not a hard cut-off in μ is that the SMG lensed by the cluster Abell 2218 has been estimated to have a (combined) amplification of $\simeq 45$ (Kneib et al. 2004). However, since there is currently only vague size information for the submm-bright regions of SMGs, there are no strong constraints on the maximum amplifications that are possible, nor on the shape of any distribution at the high μ end. At this point we believe this should be regarded as an empirical question that can only be answered by future high-resolution studies with instruments such as ALMA.

Another potential source of systematic uncertainty lies in the fact that there is only one Millennium Simulation, and it was not carried out for the currently best-fitting cosmological model. In particular the value of σ_8 used (the normalization at a scale of $8 h^{-1} \text{Mpc}$) was 0.9, while the *WMAP5* value is more like 0.8 (Dunkley et al. 2008). A smaller normalization can have a significant effect in reducing the incidence of strong lensing (e.g., Li et al. 2007; Fedeli et al. 2008). However, it is difficult to assess precisely what affect this might have on our estimates, for several reasons. Firstly, the full simulations are not available for other models. Secondly, there are other differences in the current best-fitting model, e.g. Ω_M and the primordial fluctuation slope, n (a red tilt means there are *lower* fluctuations at galaxy and group scales than in the Millennium simulation). And finally, there is still some uncertainty about the precise value of σ_8 , with the statistics of giant arcs suggesting that higher values may be a better fit (e.g., Li et al. 2007; Fedeli et al. 2008).

5.2 Source counts

As already discussed, we have taken the shallowest power-law consistent with the SHADES data as found in Coppin et al. (2006) and used that as an upper estimate on the

source counts at the bright end. At high flux densities, this upper estimate and our best guess Schechter function give significantly different results, with the ‘maximal’ counts providing the lower estimate for lensing effects.

It is possible that the observed counts already include some magnification bias. This being the case, our estimation of the expected number of bright sources will be too high, since these already amplified objects will be lensed further by our procedure in Section 4. To attempt to compensate for this, we looked at how the slope of the differential number counts changes when lensing is applied *only* at the flux densities where the data exist. Using the Schechter function, we found a negligible change, from which we conclude that lensing effects in this region are too small to change our results. However, for the broken power-law, the slope after the break (β in equation 7) is much more sensitive to changes introduced by lensing. Above the knee, Coppin et al. (2006) found $\beta = 5.1 \pm 0.9$. Fitting equation 7 to the lensed source counts for $S_{\text{obs}} \lesssim 25$, where the counts still follow a broken power-law and SHADES data exist, we find $\beta = 4.9$. This is still well within the uncertainty in the original broken power-law. In particular, the limit of $N(> 22 \text{ mJy}) < 17 \text{ deg}^{-2}$ found by Coppin et al. (2006) is maintained by the maximal broken power-law even after lensing.

We have been making the simplifying assumption that the *shape* of the submm counts is independent of redshift, even though the amount of lensing might follow a particular source redshift distribution. The main difficulty in carrying out estimates within more complicated models is that there are only relatively weak constraints on how the shape of the counts might vary with redshift. The best available evidence comes from a study of luminosity evolution among SMGs in the GOODS-North field by Wall, Pope & Scott (2008), which builds on earlier suggestions that the brightest SMGs tend to be at higher redshift. This appears to run counter to the idea of hierarchical clustering, except of course it is most likely complications with the baryons within galaxy formation that lead to this ‘down-sizing’. Wall et al. (2008) find evidence for 2 populations separated in luminosity, each having a different luminosity function slope and redshift dependence. To the extent that the negative K -correction makes up for distance dimming for SMGs, the submm flux density is a proxy for luminosity, with the break occurring near 5 mJy: fainter SMGs have a shallower slope and evolve more gently; brighter SMGs have a steeper slope and evolve more strongly with redshift. Using this approximation we find that the phenomenological models of Wall et al. (2008) do indeed lead to SMG counts which vary with redshift. However, the results are (within the fairly wide error bars) consistent with our ‘maximal’ model.

At the moment the available SMG data involve modest sample sizes, limited dynamic range and incomplete redshift information. As more is learned about how the counts evolve with redshift it will be possible to carry out more accurate calculations of the lensing effects.

6 COMPARISON WITH AN EVOLUTIONARY MODEL

A short-coming of our analysis is the assumption of a fixed shape for the source counts at all redshifts. Naive expecta-

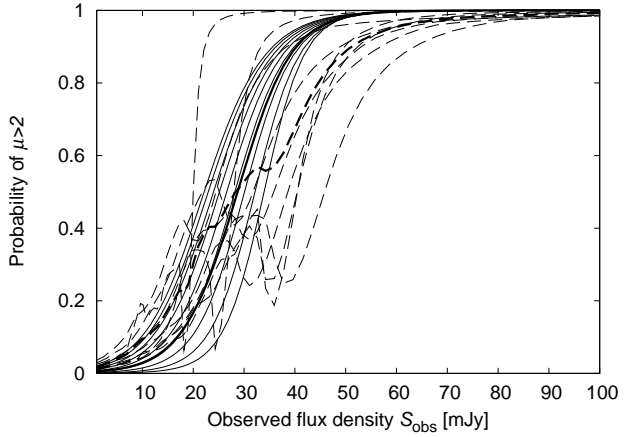


Figure 10. Dashed lines are the fraction of dN/dS_{obs} due to magnifications greater than 2 using the model from Appendix A in redshift bins of $\Delta z = 0.5$ for $0.5 < z < 5.0$. Solid lines are from the same redshift intervals using the Schechter function. The thick lines are the average over all redshifts.

tions for galaxy formation are that the most extreme SMGs would be rarer at high redshift. However, the idea of ‘down-sizing’ has been shown to apply to SMGs (Wall, Pope & Scott 2008), making the ‘hyper-LIRGs’ more prevalent at earlier times. Hence, to properly assess these effects requires a more detailed model which includes the evolution of SMGs. We choose a particular set of simulations based on the local far-infrared colour-luminosity distribution described in Chapin, Hughes & Aretxaga (2009) including evolution that reproduces the observed 850 μm source counts and redshift distribution (see the complete description in Appendix A). However, since the existing empirical information is so meager, the model’s behaviour at high redshift can only be considered as indicative. Moreover, since the model is based on a particular simulation, then it is limited for rare objects at the bright end. Nevertheless, its use should enable us to assess the effect on our estimates of allowing the number count shape to vary as a function of redshift in a way which is consistent with current data.

The simulation we utilise contains over 8 million sources between $z = 0$ and 5. We divided these sources into bins of width $\Delta z = 0.5$ and determined the differential source counts dN/dS for each bin, to which we could apply the lensing probabilities in the same way as before. The probability of a lensing event as a function of S_{obs} is shown in Fig. 10, and compared to the Schechter function using the same redshift bins.

It can be noted that the evolutionary model produces considerably more variation in lensing probability compared to the analytical Schechter function. Nonetheless, the probability is still greater than about 0.3 for any object with an observed flux greater than about 20 mJy, which is comparable to the results we found for a single counts shape. For dimmer objects, where we may need to be conservative about what sources deserve closer attention, the chances of a lensing event are actually slightly better with the evolutionary model. So the conclusion is that although our analytical approximation misses some of the structure in the redshift distribution of SMGs, the end results are quite similar. Still, this should be considered as yet another potential source of

uncertainty in the lensing predictions, and further motivation for gathering data which can distinguish among details of the models.

7 DISCUSSION AND CONCLUSIONS

We can use our study to make approximate predictions for upcoming submm surveys. There are several relevant instruments, but we focus on the surveys which are planned with the SCUBA-2 instrument (Holland et al. 2006) on the James Clerk Maxwell Telescope. There are 2 relevant $850\ \mu\text{m}$ programmes: the SCUBA-2 Cosmology Legacy Survey, S2CLS; and the SCUBA-2 ‘All Sky’ Survey, SASSy (Thompson et al. 2007).

We have also carried out estimates for surveys at shorter wavelengths, of the sort which might be performed with the $450\ \mu\text{m}$ array of SCUBA-2, or the SPIRE instrument on the *Herschel* satellite (operating at 250, 350 and $500\ \mu\text{m}$). While it is clear that there may be many examples of strong lenses in such wide surveys, the fraction of bright sources which are lensed is significantly lower than at longer wavelengths. If one wants to find such ‘monsters’, either as probes of line-of-sight structure or for their own intrinsic value, then one should turn to ground-based surveys in the $850\ \mu\text{m}$ or $\sim 1\ \text{mm}$ windows.

The S2CLS plans to map approximately $20\ \text{deg}^2$ to an RMS of $0.7\ \text{mJy}$. From our number counts model we estimate that there will be about 96, 44 and 27 sources detected with $S > 20$, 25 and $30\ \text{mJy}$, respectively. The total number of sources above these flux limits which have $\mu > 2$ will be about 15 (with most of them at the high flux end) using our best estimate from the Schechter function number counts. The numbers change only slightly over this flux density range, due to the probability of lensing increasing faster than the decrease in source counts. Above $35\ \text{mJy}$ the number of expected lensed sources declines steadily. The lensed fractions are considerably smaller using our ‘maximal’ counts model, as can be seen by referring to Fig. 6.

There will of course always be bright sources which have negligible lensing – hence one would like to know how bright to go before the probability of strong lensing is significant. This can be determined using Fig. 6. If one is prepared to accept a 1 in 3 chance of a source being strongly lensed, then one should select sources observed with $S \gtrsim 25\ \text{mJy}$. If one would like the chance to be 1 in 2, then that flux rises to about $30\ \text{mJy}$.

What would one do with such sources in practice? Since strong lensing is likely to come from either a galaxy cluster, or a massive galaxy, then the existence of strong lensing implies strongly clustered structure along that line of sight. Hence for each sufficiently bright source one would use follow-up observations at other wavelengths to try to establish whether strong lensing was likely, and then to see if one could find the structure which was responsible for the lensing. Multiple images or distorted morphologies of optical counterparts would be ways of determining that lensing was taking place – these would naturally show up as part of the procedure for trying to determine counterparts in deep data at other wavelengths. For SMGs where lensing was strongly suspected, one would target the area to search for the presence of structure along the line of sight, either with X-ray,

Sunyaev-Zel’dovich or ‘red cluster sequence’ observations. The advantage of this approach is that the high redshift of the SMG sources means that it should be feasible to find cluster (or proto-cluster) lenses at higher redshifts than are easy to achieve with most other techniques. Of course, the selection effects for clusters found in this way may be complicated to quantify. Nevertheless, building up samples of $z > 1$ clusters is sufficiently important for understanding structure formation (as well as constraining dark energy, etc.), that it is worth using every available method.

SASSy is designed to make a shallow $850\ \mu\text{m}$ map over approximately $4,000\ \text{deg}^2$, or one tenth of the sky, with the possibility of extension to a larger area later. The RMS of the maps is planned to be around $30\ \text{mJy}$, so that a robust 5σ catalogue will have a limit around $150\ \text{mJy}$. It may also be possible to reduce this to nearer to $100\ \text{mJy}$ using targeted repeat observations for peaks in the maps.

The procedure for identifying strongly lensed sources in SASSy may be a little different than for S2CLS, and because of the brighter flux densities, the level of uncertainty in predictions of the number of lensed sources will be considerably higher. These predictions depend strongly on the counts model, the normalization of the high amplification tail of the lensing PDF, as well as the amplification cut-off imposed by the finite source size for SMGs. Since there are still huge uncertainties in all of these factors, the expectations for SASSy cover a wide range of possibilities.

Using the optimistic limit of $100\ \text{mJy}$ for SASSy, the unlensed model counts give approximately 1200 sources for the SASSy catalogue. Many of these will be in the ‘Euclidean counts’ regime, and hence should be relatively easy to eliminate as lensing candidates. These will often be already well-known galaxies, with others typically being in the *IRAS*, *Akari* or radio catalogues. Colours (e.g., $850\ \mu\text{m}$ to radio) can be used to distinguish objects which are likely to be at higher redshift and hence have a higher likelihood of being lensed; such methods will also be necessary to eliminate Galactic clouds. Our best lensing estimate yields a total of 1000 sources in SASSy with lensing amplification $\mu > 2$, with most of them being much more strongly lensed than this limit. We expect that these extremely lensed sources will be fairly easy to distinguish from relatively nearby, intrinsically bright galaxies, and hence the chances of there being structure along the line of sight to such candidates will be very high. Follow-up of these SMGs at other wavelengths will also be easy, since they should be at least an order of magnitude brighter than the typical SCUBA sources which have been followed up in the past.

8 ACKNOWLEDGMENTS

We would like to thank Alexandra Pope for many helpful discussions during the course of this work. Neal Dalal and Mattia Negrello provided useful feedback on an early draft of this paper. We also thank Ranga-Ram Chary for providing his submillimetre galaxy models to us. The models of Lagache et al. are freely available online¹. This work was sup-

¹ <http://www.ias.u-psud.fr/irgalaxies/Model/>

ported by the Natural Sciences and Engineering Research Council of Canada.

REFERENCES

- Aretxaga I., Hughes D. H., Coppin K., Mortier A. M. J., Wagg J., Dunlop J. S., Chapin E. L., Eales S. A., Gaztañaga E., Halpern M., Ivison R. J., van Kampen E., Scott D., Serjeant S., Smail I., 2007, *MNRAS*, 379, 1571
- Bartelmann M., Steinmetz M., Weiss A., 1995, *A&A*, 297, 1
- Bartelmann M., Weiss A., 1994, *A&A*, 287, 1
- Blain A. W., Longair M. S., 1993, *MNRAS*, 264, 509
- Blain A. W., Smail I., Ivison R. J., Kneib J.-P., Frayer D. T., 2002, *Phys. Rep.*, 369, 111
- Borys C., Blain A. W., Dey A., Le Floc'h E., Jannuzi B. T., Barnard V., Bian C., Brodwin M., Menéndez-Delmestre K., Thompson D., Brand K., Brown M. J. I., Dowell C. D., Eisenhardt P., Farrah D., 2006, *ApJ*, 636, 134
- Borys C., Chapman S., Donahue M., Fahlman G., Halpern M., Kneib J.-P., Newbury P., Scott D., Smith G. P., 2004, *MNRAS*, 352, 759
- Chapin E. L., Hughes D. H., Aretxaga I., 2009, *MNRAS*, pp 76+
- Chapman S. C., Blain A. W., Ivison R. J., Smail I. R., 2003, *Nature*, 422, 695
- Chapman S. C., Blain A. W., Smail I., Ivison R. J., 2005, *ApJ*, 622, 772
- Chary R., Elbaz D., 2001, *ApJ*, 556, 562
- Coppin K., Chapin E. L., Mortier A. M. J., Scott S. E., Borys C., Dunlop J. S., Halpern M., Hughes D. H., Pope A., Scott D., Serjeant S., Wagg J., Alexander D. M., Almaini O., Aretxaga I., 2006, *MNRAS*, 372, 1621
- Courbin F., Saha P., Schechter P. L., 2002, in Courbin F., Minniti D., eds, *Gravitational Lensing: An Astrophysical Tool Vol. 608 of Lecture Notes in Physics*, Berlin Springer Verlag, Quasar Lensing. pp 1–54
- Dole H., Gispert R., Lagache G., Puget J.-L., Bouchet F. R., Cesarsky C., Ciliegi P., Clements D. L., Dennefeld M., Désert F.-X., Elbaz D., Franceschini A., Guiderdoni B., 2001, *A&A*, 372, 364
- Dole H., Le Floc'h E., Pérez-González P. G., Papovich C., Egami E., Lagache G., Alonso-Herrero A., Engelbracht C. W., Gordon K. D., Hines D. C., Krause O., Misselt K. A., 2004, *ApJS*, 154, 87
- Dunkley J., Spergel D. N., Komatsu E., Hinshaw G., Larson D., Nolta M. R., Odegard N., Page L., Bennett C. L., Gold B., Hill R. S., Jarosik N., Weiland J. L., Halpern M., Kogut A., Limon M., Meyer S. S., Tucker G. S., Wollack E., Wright E. L., 2008, *ArXiv e-prints*
- Dunlop J. S., McLure R. J., Yamada T., Kajisawa M., Peacock J. A., Mann R. G., Hughes D. H., Aretxaga I., Muxlow T. W. B., Richards A. M. S., Dickinson M., Ivison R. J., Smith G. P., Smail I., Serjeant S., Almaini O., Lawrence A., 2004, *MNRAS*, 350, 769
- Dunne L., Eales S., Edmunds M., Ivison R., Alexander P., Clements D. L., 2000, *MNRAS*, 315, 115
- Fedeli C., Bartelmann M., Meneghetti M., Moscardini L., 2008, *A&A*, 486, 35
- Fixsen D. J., Dwek E., Mather J. C., Bennett C. L., Shafer R. A., 1998, *ApJ*, 508, 123
- Granato G. L., Silva L., Monaco P., Panuzzo P., Salucci P., De Zotti G., Danese L., 2001, *MNRAS*, 324, 757
- Hilbert S., White S. D. M., Hartlap J., Schneider P., 2007, *ArXiv Astrophysics e-prints*, 382, 121
- Hilbert S., White S. D. M., Hartlap J., Schneider P., 2008, *MNRAS*, 386, 1845
- Holland W., MacIntosh M., Fairley A., Kelly D., Montgomery D., Gostick D., Atad-Ettinger E., Ellis M., Robson I., Hollister M., Woodcraft A., 2006, in *Millimeter and Submillimeter Detectors and Instrumentation for Astronomy III*. Edited by Zmuidzinas, Jonas; Holland, Wayne S.; Withington, Stafford; Duncan, William D. Vol. 6275 of *Presented at the Society of Photo-Optical Instrumentation Engineers (SPIE) Conference, SCUBA-2: a 10,000-pixel submillimeter camera for the James Clerk Maxwell Telescope*
- Ivison R. J., Smail I., Frayer D. T., Kneib J.-P., Blain A. W., 2001, *ApJL*, 561, L45
- Ivison R. J., Smail I., Le Borgne J.-F., Blain A. W., Kneib J.-P., Bezecourt J., Kerr T. H., Davies J. K., 1998, *MNRAS*, 298, 583
- Jain B., Seljak U., White S., 2000, *ApJ*, 530, 547
- Keeton C. R., Kuhlen M., Haiman Z., 2005, *ApJ*, 621, 559
- Kneib J.-P., Ellis R. S., Smail I., Couch W. J., Sharples R. M., 1996, *ApJ*, 471, 643
- Kneib J.-P., van der Werf P. P., Kraiberg Knudsen K., Smail I., Blain A., Frayer D., Barnard V., Ivison R., 2004, *MNRAS*, 349, 1211
- Kochanek C. S., 2006, in Meylan G., Jetzer P., North P., Schneider P., Kochanek C. S., Wambsganss J., eds, *Saas-Fee Advanced Course 33: Gravitational Lensing: Strong, Weak and Micro Part 2: Strong gravitational lensing*. pp 91–268
- Lagache G., Dole H., Puget J.-L., 2003, *MNRAS*, 338, 555
- Lagache G., Dole H., Puget J.-L., Pérez-González P. G., Le Floc'h E., Rieke G. H., Papovich C., Egami E., Alonso-Herrero A., Engelbracht C. W., Gordon K. D., Misselt K. A., Morrison J. E., 2004, *ApJS*, 154, 112
- Lewis G. F., Chapman S. C., Helou G., 2005, *ApJ*, 621, 32
- Li G. L., Mao S., Jing Y. P., Lin W. P., Oguri M., 2007, *MNRAS*, 378, 469
- Navarro J. F., Frenk C. S., White S. D. M., 1997, *ApJ*, 490, 493
- Negrello M., Perrotta F., González J. G.-N., Silva L., de Zotti G., Granato G. L., Baccigalupi C., Danese L., 2007, *MNRAS*, 377, 1557
- Perrotta F., Baccigalupi C., Bartelmann M., De Zotti G., Granato G. L., 2002, *MNRAS*, 329, 445
- Perrotta F., Magliocchetti M., Baccigalupi C., Bartelmann M., De Zotti G., Granato G. L., Silva L., Danese L., 2003, *MNRAS*, 338, 623
- Pope A., Borys C., Scott D., Conselice C., Dickinson M., Mobasher B., 2005, *MNRAS*, 358, 149
- Pope A., Scott D., Dickinson M., Chary R.-R., Morrison G., Borys C., Sajina A., Alexander D. M., Daddi E., Frayer D., MacDonald E., Stern D., 2006, *MNRAS*, 370, 1185
- Schneider P., Ehlers J., Falco E. E., 1992, *Gravitational Lenses*. Springer-Verlag Berlin
- Smail I., Smith G. P., Ivison R. J., 2005, *ApJ*, 631, 121
- Springel V., White S. D. M., Jenkins A., Frenk C. S., Yoshida N., Gao L., Navarro J., Thacker R., Croton D., Helly J., Peacock J. A., Cole S., Thomas P., Couchman

- H., Evrard A., Colberg J., Pearce F., 2005, *Nature*, 435, 629
- Swinbank A. M., Smith J., Bower R. G., Bunker A., Smail I., Ellis R. S., Smith G. P., Kneib J.-P., Sullivan M., Allington-Smith J., 2003, *ApJ*, 598, 162
- Thompson M. A., Serjeant S., Jenness T., Scott D., Ashdown M., Brunt C., Butner H., Chapin E., Chrysostomou A. C., Clark J. S., Clements D., Collett J. L., Coppin K., Coulson I. M., Dent W. R. F., 2007, *ArXiv e-prints*
- Wall J. V., Pope A., Scott D., 2008, *MNRAS*, 383, 435
- Wambsganss J., 1992, *ApJ*, 386, 19
- Wambsganss J., Ostriker J. P., Bode P., 2008, *ApJ*, 676, 753
- Wang Y., Holz D. E., Munshi D., 2002, *ApJL*, 572, L15
- Wu J. M., Chiueh T., 2006, *ApJ*, 639, 695
- Younger J. D., Fazio G. G., Huang J.-S., Yun M. S., Wilson G. W., Ashby M. L. N., Gurwell M. A., Lai K., Peck A. B., Petitpas G. R., Wilner D. J., Iono D., Kohno K., Kawabe R., Hughes D. H., Aretxaga I., 2007, *ArXiv e-prints*, 708
- Yun M. S., Reddy N. A., Condon J. J., 2001, *ApJ*, 554, 803

APPENDIX A: EVOLUTIONARY MODEL

The evolutionary model used to determine 850 μm counts as a function of redshift combines the local measurement of the joint far-IR colour-luminosity distribution, $\Phi(L, C)$ (L is the 42.5–122.5 μm far-IR luminosity, and C is the logarithm of the 60/100 μm flux density ratio) presented in Chapin et al. (2009), with a two-population evolutionary scenario similar in style to the model of Lagache et al. (2003, 2004), consisting of lower-luminosity ‘normal’ galaxies, and higher-luminosity star-bursting galaxies. The constraints for this model are the source counts at 850 μm (Coppin et al. 2006), and 170/160 μm (Dole et al. 2001, 2004), and the redshift distributions of 850 μm sources from Chapman et al. (2005). In addition we verify that the integrated contribution to the IR background in the range 850–160 μm does not exceed that measured by *COBE* (Fixsen et al. 1998).

First, similar to Yun et al. (2001), we approximate the local far-IR luminosity function by the superposition of two Schechter functions, $\phi(L) = \rho_*(L/L_*)^\alpha \exp(-L/L_*)$. For the lower-luminosity objects $\rho_* = 2.3 \times 10^{-3} \text{ Mpc}^{-3} \text{ dex}^{-1}$ and $L_* = 2.3 \times 10^{10} L_\odot$, while for the higher-luminosity objects $\rho_* = 2.3 \times 10^{-5} \text{ Mpc}^{-3} \text{ dex}^{-1}$ and $L_* = 2.2 \times 10^{11} L_\odot$. A value of $\alpha = -0.5$ is adopted for both populations. The two components are compared with the original form of Chapin et al. (2009) in Figure A1. The full local colour-luminosity distribution for each of these populations, $\Phi_1(L, C)$ and $\Phi_2(L, C)$ are then constructed by multiplying the respective Schechter functions by the conditional colour distribution $p(C|L)$, as defined in Equations 8–10 in Chapin et al. (2009) and using coefficients for the ‘dual power-law luminosity function’ fit.

The ‘normal’ galaxy population is evolved in redshift using a combination of density and luminosity evolution, $\Phi_1(L, C, z) = g(z)\Phi_1[L/h(z), C]$. For the density evolution we use the form $g(z) = (1+z)^{3/2} \text{sech}^2[b \ln(1+z) - c] \cosh^2 c$ from Lewis et al. (2005), since the 2-parameter family of curves smoothly describes a wide range of scenarios involving a steep rise with a gradual fall. We adopt coefficients $b = 4.5$ and $c = 1.6$. For the luminosity evolution $h(z)$ grows

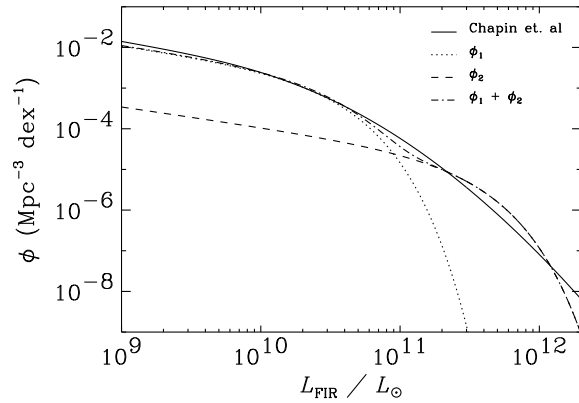


Figure A1. The local 42.5–122.5 μm far-IR luminosity function from Chapin et al. (2009) expressed as the superposition of a low-luminosity ‘normal’ galaxy population, $\phi_1(L)$, and a high-luminosity starburst population, $\phi_2(L)$, each parameterized with Schechter functions.

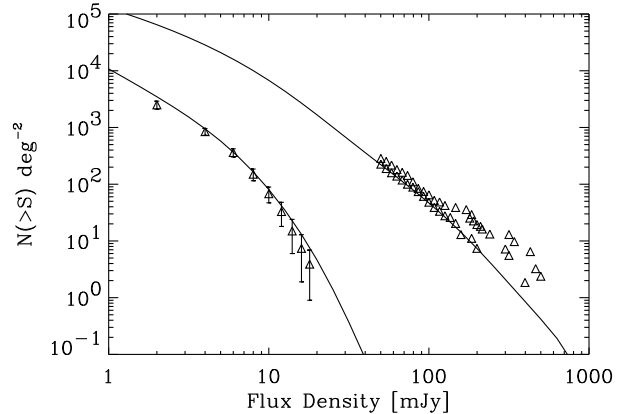


Figure A2. Observed integral source counts at 850 μm (triangles with error bars, Coppin et al. 2006) and at 170/160 μm (triangles without error bars, Dole et al. 2001, 2004). The model predictions are given by the solid lines. For the purposes of this comparison the 170 μm data are also assumed to be at 160 μm (which is a reasonable approximation given the proximity in wavelength).

as $(1+z)^{2.5}$ up to $z = 2.0$, remains constant to $z = 4.0$, and there are no more galaxies at higher redshifts. The starburst galaxy population is defined using pure luminosity evolution, $\Phi_2(L, C, z) = \Phi_2[L/g(z), C]$, where $g(z)$ is the same parameterization used for density evolution of the low-luminosity population, with $b = 1.5$ and $c = 1.3$.

Within this model the colour-luminosity correlation undergoes the same luminosity evolution as the luminosity functions for each population. It was shown in Chapin et al. (2009) that such evolution can explain the observed temperatures for a sample of 850 μm -selected galaxies at redshifts $z > 1$.

SED templates are required to calculate flux densities for particular galaxies with luminosities L and far-IR colours C drawn from the evolving distribution. Since we only consider data in the observed wavelength range 850–

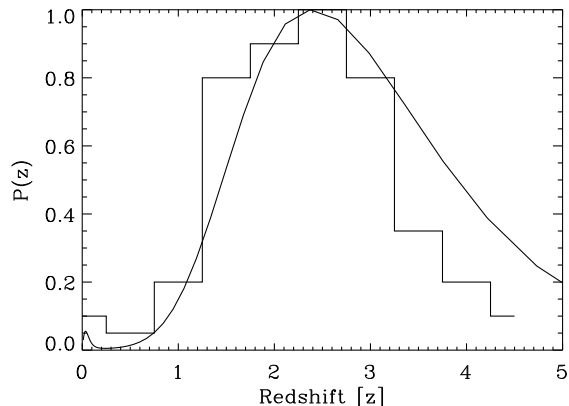


Figure A3. The observed peak-normalized redshift distribution of 850 μm sources corrected for selection effects (histogram) from Chapman et al. (2005), compared with the model prediction (solid line) for sources with $S_{850} > 5 \text{ mJy}$. This flux limit approximates that of the SCUBA surveys from which the sources were selected for the redshift survey.

160 μm we are free to use a simple modified blackbody SED, $S_\nu \propto \nu^\beta B_\nu(T)$, as there is no significant influence on the shape from hotter dust components, or complicated features related to AGN activity or polycyclic aromatic hydrocarbons in the mid-infrared. As in Chapin et al. (2009) we adopt $\beta = 1.5$ such that C maps directly to an effective dust temperature T .

The model predictions for 850 and 160 μm source counts are shown in Figure A2, along with existing measurements, demonstrating the agreement across this broad range in wavelengths. In Figure A3 we compare the model redshift distribution for 850 μm -selected sources brighter than 5 mJy compared with the redshift survey of Chapman et al. (2005), also exhibiting good agreement.

With this model set up to be consistent with current knowledge of the local luminosity function, submm number counts and redshift distributions, we can use a realization of it to generate a simulated source catalogue for studying the effects of redshift evolution on the lensing statistics.

This paper has been typeset from a \LaTeX file prepared by the author.